JOC Article

# Molecular Rotors as Simple Models to Study Amide NH−Aromatic Interactions and Their Role in the Folding of Peptide-like Structures

Ignacio Alfonso,*,† M. Isabel Burguete, Francisco Galindo, Santiago V. Luis,* and Laura Vigara

*Departamento de Química Inorgánica y Orgánica, UAMOA, Universidad Jaume I, CSIC, Campus del Riu Sec, Avenida Sos Baynat, s/n, E-12071, Castellón, Spain*

*iarqob@iiqab.csic.es; luiss@qio.uji.es*

*Received July 16, 2007*

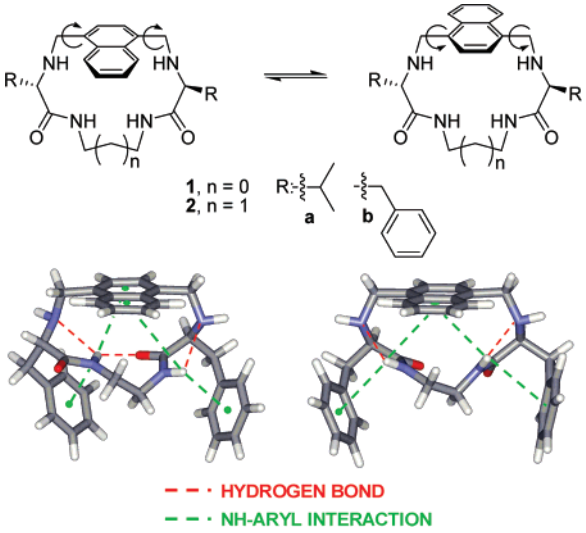


The conformational behavior of designed macrocyclic naphthalenophanes (**1a**,**b** and **2a**,**b**) derived from amino acids (Phe and Val) has been used for studying NH···$\pi$ interactions. The cycles having 16- and 17-membered rings showed a dynamic process within the NMR time scale, produced by the flipping of the aromatic naphthalene moiety with respect to the macrocyclic main plane. We used the temperature dependence of $^1$H NMR to obtain activation parameters of the energetic barrier for the process (variable temperature NMR and line shape analysis). The rate of the movement clearly depends on the macrocyclic ring size and, more interestingly, on the nature of the peptidomimetic side chain, the energetic barrier being higher for the compounds bearing aromatic side chains. A largely negative entropic contribution to the free energy of activation was observed, with clear differences due to the side chain nature. Molecular modeling studies suggest that the aromatic rings interact with intramolecularly H-bonded amide NH groups, protecting them from solvation and thus leading to a larger unfavorable activation entropy. This NH···$\pi$ interaction has been exploited for the preparation of new systems (**1c** and *meso*-**1b**) with designed conformational preferences, in which aromatic rings tend to fold over amide NH groups. Thus, these minimalistic molecular rotors have served us as simple model systems for the study of NH···$\pi$ interactions and their implication in the folding of peptide-like molecules.

## Introduction

Models are very attractive to chemists, as they allow understanding of intrinsically complicated biological systems at the molecular level.[1] Despite the obvious problem of oversimplification, we can obtain important information about the source and characteristics of weak interactions, such as hydrogen bonding, cation−$\pi$ interactions, or solvophobic

* Corresponding authors. Phone: +34 964728239; fax: +34 964728214.
† Present address: Department of Biological Organic Chemistry, IIQAB-CSIC, Jordi Girona 18-26, E-08034, Barcelona, Spain.

(1) For a very recent discussion on this topic, see: Kool, E. T.; Waters, M. L. *Nat. Chem. Biol.* **2007**, *3*, 70−73.

10.1021/jo701552b CCC: $37.00 
Published on Web 09/21/2007

contacts. Among others, hydrogen bonds implicating both the $\pi$-cloud of aromatic systems and amide NH bonds have been deeply studied in the past decade,[2] as they are present in many proteins[3] and peptides[4] and have been used for molecular recognition in synthetic receptors.[5] However, the use of these noncovalent contacts for conformational control[6] and the development of model systems for studying the process[7] have been less exploited. The understanding of these noncovalent interactions is of great importance, as there are some biological processes that are closely related, such as protein binding to specific ligands[8] or the regulation of molecular recognition of DNA.[9]

On the other hand, amino acid derived macrocyclic compounds have recently attracted much attention in the fields of synthetic,[10] bioorganic,[11] medicinal,[12] and supramolecular chemistry.[13] Their cyclic structure usually confers on them a three-dimensional organization of the amino acid residues in a preferred conformation,[14] allowing them to host small molecules and ions,[15] with interesting potentials in molecular recognition or in the design of new chemosensors.[16] Thus, the conformationally well-defined disposition of functional groups make them ideal probes for the study of noncovalent interactions in relation to solvent exposure and folding properties and, consequently, for designing model systems. Regarding that, we have recently reported on the study of conformational properties of macrocyclic peptidomimetic cyclophanes containing a *p*-phenylene unit.[17] The energetic barrier for the rotation of the aromatic ring with respect to the macrocyclic main plane showed a close relationship with the intramolecular H-bond pattern and the solvent accessibility to the pseudo-peptidic moiety. These properties were exploited for the description of a methanol-dependent molecular rotor, a simple device that was used as a proof-of-concept simple model. Additionally, the effect of the aromatic rings of the side chains was correlated to the ability

(2) (a) Meyer, E. A.; Castellano, R. K.; Diederich, F. *Angew. Chem., Int. Ed.* **2003**, *42*, 1210−1250. (b) Ma, J. C.; Dougherty, D. A. *Chem. Rev.* **1997**, *97*, 1303−1324.

(3) (a) Steiner, T.; Koellner, G. *J. Mol. Biol.* **2001**, *305*, 535−557. (b) Singh, J.; Thornton, J. M. *J. Mol. Biol.* **1990**, *211*, 595−615. (c) Burley, S. K.; Petsko, G. A. *Adv. Protein Chem.* **1988**, *39*, 125−189. (d) Burley, S. K.; Petsko, G. A. *FEBS Lett.* **1986**, *203*, 139−143.

(4) (a) Mahalakshmi, R.; Raghothama, S.; Balaram, P. *J. Am. Chem. Soc.* **2006**, *128*, 1125−1138. (b) Harini, V. V.; Aravinda, S.; Rai, R.; Shamala, N.; Balaram, P. *Chem.—Eur. J.* **2005**, *11*, 3609. (c) Sengupta, A.; Mahalakshmi, R.; Shamala, N.; Balaram, P. *J. Peptide Res.* **2005**, *65*, 113−129. (d) Chin, W.; Mons, M.; Dognon, J.-P.; Mirasol, R.; Chass, G.; Dimicoli, I.; Piuzzi, F.; Butz, P.; Tardivel, B.; Compagnon, I.; von Helden, G.; Meijer, G. *J. Phys. Chem. A* **2005**, *109*, 5281−5288. (e) Broda, M. A.; Siodlak, D.; Rzeszotarska, B. *J. Peptide Sci.* **2005**, *11*, 235−244. (f) Toth, G.; Kover, K. E.; Murphy, R. F.; Lovas, S. *J. Phys. Chem. B* **2004**, *108*, 9287−9296. (g) Casanovas, J.; Jiménez, A. I.; Cativiela, C.; Pérez, J. J.; Alemán, C. *J. Org. Chem.* **2003**, *68*, 7088−7091. (h) Toth, G.; Watts, C. R.; Murphy, R. F.; Lovas, S. *Proteins: Struct., Funct., Genet.* **2001**, *43*, 373−381. (i) Toth, G.; Murphy, R. F.; Lovas, S. *Protein Eng.* **2001**, *14*, 543−547. (j) Toth, G.; Murphy, R. F.; Lovas, S. *J. Am. Chem. Soc.* **2001**, *123*, 11782−11790. (k) Jiménez, A. I.; Cativiela, C.; Gómez-Catalán, J.; Pérez, J. J.; Aubry, A.; París, M.; Marraud, M. *J. Am. Chem. Soc.* **2000**, *122*, 5811−5821. (l) Honda, M. S.; Kobayashi, N.; Munekata, E. *J. Mol. Biol.* **2000**, *295*, 269−278. (m) Duan, G.; Smith, V. H.; Weaver, D. F. *Int. J. Quantum Chem.* **2000**, *80*, 44−60. (n) Jiménez, A. I.; Cativiela, C.; Aubry, A.; Marraud, *J. Am. Chem. Soc.* **1998**, *120*, 9452−9459. (o) Crisma, M.; Formaggio, F.; Valle, G.; Toniolo, C.; Saviano, M.; Iacovino, R.; Zaccaro, L.; Benedetti, E. *Biopolymers* **1997**, *42*, 1−6. (p) van der Spoel, D.; van Buuren, A. R.; Tieleman, P.; Berendsen, H. J. C. *J. Biomol. NMR* **1996**, *8*, 229−238.

(5) (a) Snowden, T. S.; Bisson, A. P.; Anslyn, E. V. *J. Am. Chem. Soc.* **1999**, *121*, 6324−6325. (b) Allott, C.; Adams, H.; Bernard, P. L., Jr.; Hunter, C. A.; Rotger, C.; Thomas, J. A. *Chem. Commun.* **1998**, 2449−2450. (c) Bisson, A. P.; Lynch, V. M.; Monahan, M. C.; Anslyn, E. V. *Angew. Chem., Int. Ed.* **1997**, *36*, 2340−2342. (d) Adams, H.; Carver, F. J.; Hunter, C. A.; Osborne, N. J. *Chem. Commun.* **1996**, 2529−2530.

(6) (a) Casanovas, J.; Jiménez, A. I.; Cativiela, C.; Pérez, J. J.; Alemán, C. *J. Phys. Chem. B* **2006**, *110*, 5762−5766. (b) Hunter, C. A.; Spitaleri, A.; Tomas, S. *Chem. Commun.* **2005**, 3691−3693.

(7) (a) Hughes, R. M.; Waters, M. L. *J. Am. Chem. Soc.* **2006**, *128*, 13586−13591. (b) Hughes, R. M.; Waters, M. L. *J. Am. Chem. Soc.* **2005**, *127*, 6518−6519. (c) Tatko, C. D.; Waters, M. L. *J. Am. Chem. Soc.* **2004**, *126*, 2028−2034. (d) Biot, C.; Buisine, E.; Rooman, M. *J. Am. Chem. Soc.* **2003**, *125*, 13988−13994. (e) Tatko, C. D.; Waters, M. L. *Protein Sci.* **2003**, *12*, 2443−2452. (f) Tsuzuki, S.; Honda, K.; Uchimaru, T.; Mikami, M.; Tanabe, K. *J. Am. Chem. Soc.* **2000**, *122*, 11450−11458.

(8) (a) Perutz, M. F. *Philos. Trans. Phys. Sci. Eng.* **1993**, *345*, 105−112. (b) Perutz, M. F.; Fermi, G.; Abraham, D. J.; Poyart, C.; Bursaux, E. *J. Am. Chem. Soc.* **1986**, *108*, 1064−1078.

(9) (a) Biot, C.; Buisine, E.; Rooman, M. *J. Am. Chem. Soc.* **2003**, *125*, 13988−13994. (b) Owen, D. J.; Ornaghi, P.; Yang, J. C.; Lowe, N.; Evans, P. R.; Ballario, P.; Neuhaus, D.; Filetici, P.; Travers, A. A. *EMBO J.* **2000**, *19*, 6141−6149. (c) Dhalluin, C.; Carlson, J. E.; Zeng, L.; He, C.; Aggarwal, A.; Zhou, M. *Nature* **1999**, *399*, 491−496.

(10) (a) Gibson, S. E.; Lecci, C. *Angew. Chem., Int. Ed.* **2006**, *45*, 1364−1377. (b) Billing, J. F.; Nilsson, U. J. *J. Org. Chem.* **2005**, *70*, 4847−4850. (c) Punna, S.; Kuzelka, J.; Wang, Q.; Finn, M. G. *Angew. Chem., Int. Ed.* **2005**, *44*, 2215−2220. (d) Cristau, P.; Martin, M.-T.; Tran Hu Dau, M.-E.; Vors, J.-P.; Zhu, J. *Org. Lett.* **2004**, *6*, 3183−3186. (e) Redman, J. E.; Wilcoxen, K. M.; Ghadiri, M. R. *J. Comb. Chem.* **2003**, *5*, 33−40. (f) Locardi, E.; Stöckle, M.; Garner, S.; Kessler, H. *J. Am. Chem. Soc.* **2001**, *123*, 8189−8196. (g) Dietrich, B.; Viout, P.; Lehn, J.-M. *Macrocyclic Chemistry*; Wiley: New York, 1993. (h) Parker, D. *Macrocycle Synthesis: A Practical Approach*; Oxford University Press: New York, 1996. (i) Vögtle, F. *Cyclophane Chemistry*; Wiley: New York, 1993.

(11) (a) Horne, W. S.; Stout, C. D.; Ghadiri, M. R. *J. Am. Chem. Soc.* **2003**, *125*, 9372−9376. (b) Fernández-López, S.; Kim, H.-S.; Choi, E. C.; Delgado, M.; Granja, J. R.; Khasanov, A.; Kraehenbuehl, K.; Long, G.; Weinberger, D. A.; Wilcoxen, K. M.; Ghadiri, M. R. *Nature* **2001**, *412*, 452−455.

(12) (a) Loughlin, W. A.; Tyndall, J. D. A.; Glenn, M. P.; Fairlie, D. P. *Chem. Rev.* **2004**, *104*, 6085−6117. (b) Reid, R. C.; Pattenden, L. K.; Tyndall, J. D. A.; Martin, J. L.; Walsh, T.; Fairlie, D. P. *J. Med. Chem.* **2004**, *47*, 1641−1651. (c) Reid, R. C.; Abbenante, G.; Taylor, S. M.; Fairlie, D. P. *J. Org. Chem.* **2003**, *68*, 4464−4471. (d) Hu, X.; Nguyen, K. T.; Verlinde, C. L. M. J.; Hol, W. G. J.; Pei, D. *J. Med. Chem.* **2003**, *46*, 3771−3774. (e) Glenn, M. P.; Pattenden, L. K.; Reid, R. C.; Tyssen, D. P.; Tyndall, J. D. A.; Birch, C. J.; Fairlie, D. P. *J. Med. Chem.* **2002**, *45*, 371−381.

(13) For some examples on related systems, see: (a) Choi, K.; Hamilton, A. D. *Coord. Chem. Rev.* **2003**, *240*, 101−110. (b) Choi, K.; Hamilton, A. D. *J. Am. Chem. Soc.* **2003**, *125*, 10241−10249. (c) Choi, K.; Hamilton, A. D. *J. Am. Chem. Soc.* **2001**, *123*, 2456−2457. (d) Somogyi, L.; Haberhauer, G.; Rebek, J., Jr. *Tetrahedron* **2001**, *57*, 1699−1708. (e) Conn, M. M.; Rebek, J., Jr. *Chem. Rev.* **1997**, *97*, 1647−1668.

(14) (a) Bru, M.; Alfonso, I.; Burguete, M. I.; Luis, S. V. *Tetrahedron Lett.* **2005**, *46*, 7781−7785. (b) Reyes, S. J.; Burgess, K. *Tetrahedron: Asymmetry* **2005**, *16*, 1061−1069. (c) Singh, Y.; Stoermer, M. J.; Lucke, A. J.; Guthrie, T.; Fairlie, D. P. *J. Am. Chem. Soc.* **2005**, *127*, 6563−6572. (d) Velasco-Torrijos, T.; Murphy, P. V. *Org. Lett.* **2004**, *6*, 3961−3964. (e) Mann, E.; Kessler, H. *Org. Lett.* **2003**, *5*, 4567−4570. (f) Singh, Y.; Stoermer, M. J.; Lucke, A. J.; Glenn, M. P.; Fairlie, D. P. *Org. Lett.* **2002**, *4*, 3367−3370. (g) Sastry, T. V. R. S.; Banerji, B.; Kumar, S. K.; Kunwar, A. C.; Das, J.; Nandy, J. P.; Iqbal, J. *Tetrahedron Lett.* **2002**, *43*, 7621−7625. (h) Reid, R. C.; Kelso, M. J.; Scanlon, M. J.; Fairlie, D. P. *J. Am. Chem. Soc.* **2002**, *124*, 5673−5683.

(15) (a) Bru, M.; Alfonso, I.; Burguete, M. I.; Luis, S. V. *Angew. Chem., Int. Ed.* **2006**, *45*, 6155−6159. (b) Heinrichs, G.; Kubic, S.; Lacour, J.; Vial, L. *J. Org. Chem.* **2005**, *70*, 4498−4501. (c) Otto, S.; Kubik, S. *J. Am. Chem. Soc.* **2003**, *125*, 7804−7805. (d) Heinrichs, G.; Vial, L.; Lacour, J.; Kubic, S. *Chem. Commun.* **2003**, 1252−1253. (e) Kubic, S.; Kirchner, R.; Nolting, D.; Seidel, J. *J. Am. Chem. Soc.* **2002**, *124*, 12752−12760. (f) Bitta, J.; Kubik, S. *Org. Lett.* **2001**, *3*, 2637−2640. (g) Kubik, S.; Goddard, R.; Kirchner, R.; Nolting, D.; Seidel, J. *Angew. Chem., Int. Ed.* **2001**, *40*, 2648−2651. (h) Pohl, S.; Goddard, R.; Kubik, S. *Tetrahedron Lett.* **2001**, *42*, 7555−7558. (i) Ishida, H.; Inoue, Y. *Biopolymers* **2000**, *55*, 469−478.

(16) (a) Galindo, F.; Burguete, M. I.; Vigara, L.; Luis, S. V.; Russell, D. A.; Kabir, N.; Gavrilovic, J. *Angew. Chem., Int. Ed.* **2005**, *44*, 6504−6508. (b) Galindo, F.; Burguete, M. I.; Luis, S. V. *Chem. Phys.* **2004**, *302*, 287−294. (c) Becerril, J.; Burguete, M. I.; Escuder, B.; Galindo, F.; Gavara, R.; Miravet, J. F.; Luis, S. V.; Peris, G. *Chem.—Eur. J.* **2004**, *10*, 3879−3890. (d) Galindo, F.; Becerril, J.; Burguete, M. I.; Luis, S. V.; Vigara, L. *Tetrahedron Lett.* **2004**, *45*, 1659−1662.

(17) Alfonso, I.; Burguete, M. I.; Luis, S. V. *J. Org. Chem.* **2006**, *71*, 2242−2250.

**SCHEME 1. Molecular Structures (with Atom Numbering) and Naphthalene Dynamic Process of 1a,b and 2a,b**

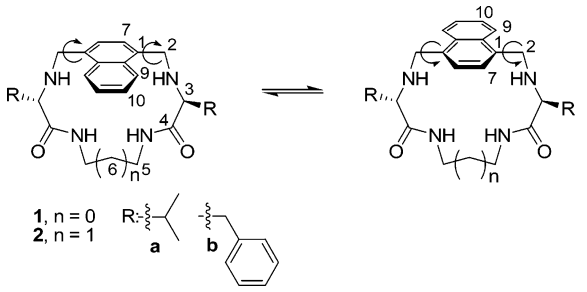


of these groups to prevent amide solvation, probably due to a stabilizing NH···$\pi$ noncovalent interaction. Intrigued by these observations, we have prepared a second generation of peptidomimetic macrocycles, implementing a naphthalene aromatic ring in their structure. Considering the behavior observed previously, these compounds will show a dynamic flipping process of the naphthalene ring within the NMR time scale (Scheme 1). Besides, the naphthalene group will have multiple effects. First of all, it will break the $C_2$ symmetry of the compounds in the slow movement regime, as the aromatic ring tends to set perpendicular to the macrocyclic plane (Scheme 1). Second, this aromatic system with an increased diamagnetic anisotropy will induce a larger anisocrony of the diastereotopic protons of the pseudo-peptidic macrocycle. Last, but not least, the aromatic surface will produce a more efficient desolvation of the intramolecularly H-bound amide NH protons. Thus, we envisioned **1a**,**b** and **2a**,**b** as good candidates for the detection of NH···$\pi$ interactions through the deep knowledge of their conformational behavior. The understanding of these processes would be valuable for the design of new molecular devices,[18] either with internal or with external control of the disposition and dynamics of some parts of the system. On the other hand, they serve as very simple models for studying the role of NH−aryl interactions in conformational flexibility and stability, in a deep relationship with solvent exclusion,[19] and, therefore, with a three-dimensional structure of biomolecules and protein folding processes.[20]

## Results and Discussion

**Variable Temperature Nuclear Magnetic Resonance (VT-NMR) Study.** For the study of the conformational process proposed in Scheme 1, we performed a $^1$H NMR analysis of **1a**,**b** and **2a**,**b** at different temperatures (VT-NMR).[21] Interestingly, due to the large diamagnetic anisotropy produced by the naphthalene ring, several proton signals of the compounds split off at temperatures below coalescence, within the slow exchange regime. This fact has allowed us to use different NMR signals as molecular probes for the study of conformational processes. A representative example is shown in Figure 1, in which **2a** showed seven signals with a typical coalescence behavior. The identity of the signals as well as the exchanging nuclei were confirmed by a set of 1-D NOESY experiments at low temperatures and are in good agreement with the dynamic flipping of the naphthalene group with respect to the macrocyclic main plane, as it would mainly affect the signals close to the C1−C2 bond. Coalescence temperatures ($T_c$) for different signals of **1a**,**b** and **2a**,**b** are given in Table 1, as well as the free energies of activation ($\Delta G^{\ddagger}$) at the coalescence temperature.[22]

By comparing the values in Table 1, very interesting trends were found. The enlargement of the macrocyclic structure by one methylene decreases the conformational energy barrier by ca. 4 kcal/mol, in reasonable agreement with reported data on polyamino cyclophanes.[17,24] Considering the data with the parent *p*-cyclophane derivatives,[17] a slightly lower rotational barrier was found for the naphthalenophanes. This apparently surprising result can be explained by steric factors. The size of the moiety passing through the macrocyclic cavity for the rotation of the phenylene and the flipping of the naphthalene moieties is essentially the same. However, the naphthalene derivatives experience an additional steric repulsion between H2 and H9 protons (see modeled structures). This interaction destabilizes the corresponding ground states and leads to a lower energetic barrier for the conformational process.

Apart from the higher conformational rigidity of the smaller cycles, an effect of the side chain nature is also noteworthy. Thus, by comparing entries 3 versus 8 and 4 versus 9 in Table 1, we can conclude that the phenylalanine derivatives lead to less flexible cycles, at least regarding the ring inversion process. This energy barrier difference is larger in the smaller macrocycles, being almost abolished for the 17-membered rings. The smooth energy gap obtained when changing $^i$Pr into Bn was

(18) For some recent revisions, see: (a) Kottas, G. S.; Clark, L. I.; Horinek, D.; Michl, J. *Chem. Rev.* **2005**, *105*, 1281−1376. (b) Sauvage, J.-P. *Chem. Commun*. **2005**, 1507−1510. (c) Mandl, C. P.; König, B. *Angew. Chem., Int. Ed.* **2004**, *43*, 1622−1624. (d) Jimenez-Molero, M. C.; Dietrich-Buchecker, C.; Sauvage, J.-P. *Chem. Commun*. **2003**, 1613−1616. (e) Balzani, V.; Credi, A.; Venturi, M. *Chem.—Eur. J.* **2002**, *8*, 5525−5530. (f) Balzani, V.; Credi, A.; Raymo, F. M.; Stoddart, J. F. *Angew. Chem., Int. Ed.* **2000**, *39*, 3348−3391.

(19) Jusuf, S.; Axelsen, P. H. *Biochemistry* **2004**, *43*, 15446−15452 and references therein.

(20) (a) Gray, R.; Trent, J. O. *Biochemistry* **2005**, *44*, 2469−2477. (b) Jourdan, M.; Searle, M. S. *Biochemistry* **2001**, *40*, 10317−10325.

(21) For some recent examples on dynamic NMR applied to conformational analysis, see: (a) Casarini, D.; Lunazzi, L.; Mancinelli, M.; Mazzanti, A. *J. Org. Chem.* **2007**, *72*, 998−1004. (b) Nygaard, S.; Leung, K. C. F.; Aprahamian, I.; Ikeda, T.; Saha, S.; Laursen, B. W.; Kim, S. Y.; Hansen, S. W.; Stein, P. C.; Flood, A. H.; Stoddart, J. F.; Jeppesen, J. O. *J. Am. Chem. Soc.* **2007**, *129*, 960−970. (c) Lunazzi, L.; Mazzanti, A.; Minzoni, M. *J. Org. Chem.* **2006**, *71*, 9297−9301. (d) Fukuhara, G.; Mori, T.; Wada, T.; Inoue, Y. *J. Org. Chem.* **2006**, *71*, 8233−8243. (e) Casarini, D.; Coluccini, C.; Lunazzi, L.; Mazzanti, A. *J. Org. Chem.* **2006**, *71*, 6248−6250. (f) Mazzanti, A.; Lunazzi, L.; Minzoni, M.; Anderson, J. E. *J. Org. Chem.* **2006**, *71*, 5474−5481. (g) Casarini, D.; Coluccini, C.; Lunazzi, L.; Mazzanti, A. *J. Org. Chem.* **2006**, *71*, 4490−4496. (h) Bogdan, N.; Grosu, I.; Benoit, G.; Toupet, L.; Ramondenc, Y.; Condamine, E.; Silaghi-Dumitrescu, I.; Ple, G. *Org. Lett.* **2006**, *8*, 2619−2622. (i) Hassner, A.; Amit, B.; Marks, V.; Gottlieb, H. E. *Eur. J. Org. Chem.* **2006**, 1256−1261. (j) Lunazzi, L.; Mazzanti, A.; Minzoni, M.; Anderson, J. E. *Org. Lett.* **2005**, *7*, 1291−1294. (k) González-Núñez, M. E.; Mello, R.; Royo, J.; Asensio, G.; Monzó, I.; Tomás, F.; García-López, J.; López-Ortiz, F. *J. Org. Chem.* **2005**, *70*, 3450−3457. (l) Lam, P. C.-H.; Carlier, P. R. *J. Org. Chem.* **2005**, *70*, 1530−1538. (m) Lunazzi, L.; Mazzanti, A.; Mizoni, M. *J. Org. Chem.* **2005**, *70*, 456−462. (n) Qadir, M.; Cobb, J.; Sheldrake, P. W.; Whittall, N.; White, A. J. P.; Hii, K. K.; Horton, P.; Hursthouse, M. B. *J. Org. Chem.* **2005**, *70*, 1545−1551. (o) Qadir, M.; Cobb, J.; Sheldrake, P. W.; Whittall, N.; White, A. J. P.; Hii, K. K.; Horton, P.; Hursthouse, M. B. *J. Org. Chem.* **2005**, *70*, 1551−1557. (p) Viñas, C.; Llop, J.; Teixidor, F.; Kivekäs, R.; Sillanpä, R. *Chem.—Eur. J.* **2005**, *11*, 1933−1941. (q) Alezra, V.; Bernardinelli, G.; Corminboeuf, C.; Frey, U.; Kündig, E. P.; Merbach, A. E.; Saudan, C. M.; Viton, F.; Weber, J. *J. Am. Chem. Soc.* **2004**, *126*, 4843−4853. (r) Rashkin, M. J.; Hughes, R. M.; Calloway, N. T.; Waters, M. L. *J. Am. Chem. Soc.* **2004**, *126*, 13320−13325.

(22) Sandström, J. *Dynamic NMR Spectroscopy*; Academic Press: London, 1982.

(23) All the line shape simulations were performed using the gNMR v4.1.0 program.

(24) (a) Burguete, M. I.; Escuder, B.; García-España, E.; López, L.; Luis, S. V.; Miravet, J. F.; Querol, M. *Tetrahedron Lett.* **2002**, *43*, 1817−1819. (b) Burguete, M. I.; Escuder, B.; García-España, E.; Luis, S. V.; Miravet, J. F. *Tetrahedron* **2002**, *58*, 2839−2846. (c) Burguete, M. I.; Escuder, B.; García-España, E.; Luis, S. V.; Miravet, J. F. *J. Org. Chem.* **1994**, *59*, 1067−1071.

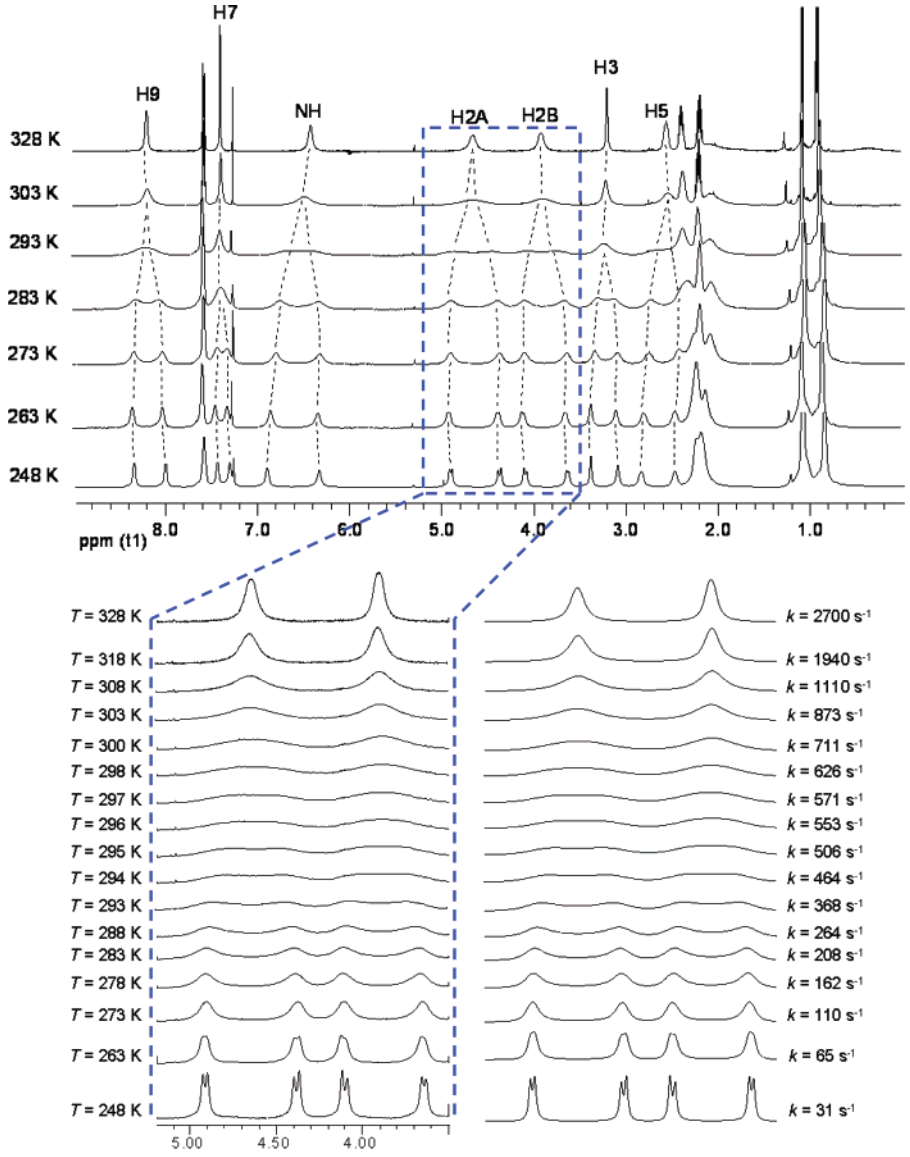


**FIGURE 1.** $^1$H NMR spectra of **2a** (500 MHz, $CDCl_3$) at selected temperatures. Atom numbering is as in Scheme 1. In the inset, the experimental (left) and simulated (right) partial NMR spectra of protons at C2 are shown. Temperatures (K) and computed exchange rates ($s^{-1}$) are also given for every trace. Simulated spectra were obtained with the gNMR program.[23]

also observed previously in related examples and was correlated to the different solvation of amide NH groups.[17] When comparing energetic barriers calculated from the coalescence of different signals of the same compound, we found a very good fitting for the larger rings. Merging different entries, we estimated an averaged $\Delta G^{\ddagger} = 13.7$ kcal/mol for **2a** (see entries 10−16 in Table 1) and $\Delta G^{\ddagger} = 14.0$ kcal/mol for **2b** (see entries 17−21 in Table 1), the individual values obtained for each proton signal being within experimental error (±0.4 kcal/mol). However, discrepancies above the experimental error were found for the smaller macrocycles (compare, for instance, entries 1 and 3−and 4 or 6 and 8− and 9 in Table 1). Interestingly, these differences are observed for signals presenting very different coalescence temperatures, which depend on both energetic barrier of the conformational process and frequency difference between exchanging nuclei at the slow exchange regime.[22] This trend suggested that $\Delta G^{\ddagger}$ is strongly dependent on the temperature, in other words, that the energetic barrier is entropically driven. To check this proposal, the activation parameters were measured by performing full line shape analyses of the protons at C2 in **1a**,**b** (Figures 2 and 3) and **2a** (Figure 1, inset). For **2b**, a serious signal overlapping prevented accurate computer simulation of the spectra. Besides, this analysis allows us to know the temperature dependence of the conformational energy barrier itself. Arrhenius activation energies ($E_a$) or enthalpic ($\Delta H^{\ddagger}$) and entropic ($\Delta S^{\ddagger}$) contributions to the free energy of activation were obtained either by ln($k$) versus 1/$T$ or Eyring plots, respectively (Table 2).[22]

As predicted, values in Table 2 show a strong temperature dependence of the free energy of activation for this conformational process.[25] Thus, the value of the entropy of activation is negative in all cases. Besides, $\Delta S^{\ddagger}$ is larger for the smaller cycles, being predominant over $\Delta H^{\ddagger}$ in its contribution to $\Delta G^{\ddagger}$. As entropy can be seen as the thermodynamic measurement of

(25) This entropic contribution has been previously reported in related systems: (a) Chang, M. H.; Masek, B. B.; Dougherty, D. A. *J. Am. Chem. Soc.* **1985**, *107*, 1124−1133. (b) Chang, M. H.; Dougherty, D. A. *J. Am. Chem. Soc.* **1983**, *105*, 4102−4103.

**TABLE 1. Frequency Difference ($\delta\nu$, Hz), Coalescence Temperature ($T_c$, K) and Energetic Barrier at $T_c$ ($\Delta G^{\ddagger}_c$, kcal/mol) for Conformational Process of Napthalenophanes 1a,b and 2a,b Using Different Proton Signals**

| entry | compd | $^1$H NMR signal | $\delta\nu^a$ (Hz) | $T_c$ (K) | $\Delta G^{\ddagger}_c$ (kcal/mol)$^{b,c}$ | solvent |
|---|---|---|---|---|---|---|
| 1 | **1a** | H9 | 23.8 | 323 | 16.4 | DMSO-$d_6$ |
| 2 | **1a** | amide−NH | 220.8 | 370 | 17.3 | DMSO-$d_6$ |
| 3 | **1a** | H2A | 200.0 | 375 | 17.6 | DMSO-$d_6$ |
| 4 | **1a** | H2B | 231.5 | 378 | 17.6 | DMSO-$d_6$ |
| 5 | **1b** | H9 | 9.4 | 343 | 18.2 | DMSO-$d_6$ |
| 6 | **1b** | H10 | 15.8 | 343 | 17.8 | DMSO-$d_6$ |
| 7 | **1b** | amide−NH | 175.8 | 383 | 18.2 | DMSO-$d_6$ |
| 8 | **1b** | H2A | 184.8 | 403 | 19.1 | DMSO-$d_6$ |
| 9 | **1b** | H2B | 251.6 | 413 | 19.3 | DMSO-$d_6$ |
| 10 | **2a** | H9 | 171.0 | 293 | 13.7 | $CDCl_3$ |
| 11 | **2a** | H7 | 64.0 | 283 | 13.8 | $CDCl_3$ |
| 12 | **2a** | amide−NH | 282.5 | 294 | 13.5 | $CDCl_3$ |
| 13 | **2a** | H2A | 265.8 | 297 | 13.6 | $CDCl_3$ |
| 14 | **2a** | H2B | 229.5 | 295 | 13.8 | $CDCl_3$ |
| 15 | **2a** | H3 | 147.5 | 287 | 13.5 | $CDCl_3$ |
| 16 | **2a** | H5 | 185.0 | 293 | 13.6 | $CDCl_3$ |
| 17 | **2b** | H9 | 97.6 | 295 | 14.2 | $CDCl_3$ |
| 18 | **2b** | amide−NH | 166.5 | 297 | 14.0 | $CDCl_3$ |
| 19 | **2b** | H2A | 240.6 | 308 | 14.3 | $CDCl_3$ |
| 20 | **2b** | H2B | 151.8 | 297 | 14.0 | $CDCl_3$ |
| 21 | **2b** | H3 | 55.2 | 280 | 13.7 | $CDCl_3$ |

[a] Measured at the low-temperature spectra. [b] Calculated using the approximated formula for $\Delta G^{\ddagger}$ at the temperature of coalescence. [c] Estimated error ±0.4 kcal/mol.

molecular disorder, the negative value of $\Delta S^{\ddagger}$ should mean that the transition state (TS) must be more ordered than the ground state (GS). This molecular order could come from a less flexible TS than the GS or from an increasing solvation from the GS to the TS. More interestingly, the effect of the side chains is mainly entropic (see entries 1 and 2 in Table 2), the $\Delta G^{\ddagger}$ value being identical for both derivatives **1a** and **1b** at 298 K. Upon heating, the very large entropic contribution to $\Delta G^{\ddagger}$ for **1b** increases the energetic barrier much more than for **1a**, highlighting their differences at the coalescence temperatures. Comparing rings of the same size, the change in the internal molecular order from the GS to the TS should be very similar; the entropic difference between **1a** and **1b** is most likely related to the solvation properties of both. These results must be carefully considered if the measurements have been performed in very different solvents but are completely correct when comparing results measured in the same solvent (entries 1 and 2 in Table 2). In these macrocyclic systems, hydrogen bonding abilities play a very important role in the conformational preferences and have to be taken into account.[17] With this regard, the amide NH chemical shifts of **1a**,**b** showed little differences when the $^1$H NMR spectra acquired either in $CDCl_3$ or in DMSO-$d_6$ were compared [$\delta$(DMSO-$d_6$) − $\delta$($CDCl_3$) = 0.49−0.51 ppm]. These data support the efficient shielding of the pseudo-peptidic moiety from solvent molecules. Accordingly, the corresponding bis-(aminoamide) portion would present an intramolecular H-bonding pattern, as initially observed with related systems.[17,26] Moreover, as the flipping of the naphthalene ring with respect to the macrocycle implies the breaking of the intramolecular H-bonging pattern, the more efficient the prevention of the solvation of the amide NH is, the larger the barrier for the ring inversion is.[17] With this rationale in mind, the larger $\Delta S^{\ddagger}$ value for **1b** than for **1a** would imply a more efficient desolvation of the amide bond in the phenylalanine derivative.

**Molecular Modeling.** For a clearer picture of the more stable conformations of these peptidomimetic naphthalenophanes, a Monte Carlo random conformational search with MMFF force field minimization was performed for every compound.[27] The global minima of energy thus obtained for every macrocycle are shown in Figure 4.

All of them showed the naphthalene moiety perpendicular to the macrocyclic main plane, in good agreement with reported crystal structures and molecular modeling studies on similar compounds.[17,26] This disposition would set the peptidomimetic chain on top of the anisotropy cone of the naphthalene ring, explaining the observed upfield shift of the corresponding signals, which is especially important for the amide NH protons. Amide protons are H-bonded to the amino nitrogens, forming five-membered rings in all the derivatives. Additionally, for the smaller cycles **1a**,**b**, there is an interesting C═O···H−N hydrogen bond, forming a seven-membered ring, which resembles the $\gamma$-turn conformation found in peptide structures.[28] On the other hand, the minima for the phenylalanine derivatives (**1b** and **2b**) tend to set the $\pi$-cloud of the aryl moieties of the side chains close to the H-bound amide protons, being especially of note for compound **1b**. This suggests the possibility of an NH···$\pi$ stabilizing interaction. Actually, measured distances on **1b** between the amide NH and the center of the closest C−C bond of the aromatic rings (2.67−3.05 Å) imply a naphthyl···amide NH···phenyl sandwich disposition. This scenario would explain the more efficient desolvation of the H-bound amide NH groups in **1b**, leading to a much larger $\Delta S^{\ddagger}$ value. We also have used molecular modeling for the qualitative visualization of the solvation differences between **1a** and **1b**. The computed solvent-accessible surfaces for both minima (see Supporting Information) showed clear differences, highlighting the more hindered accessibility of DMSO molecules to the amide groups in **1b** due to the presence of the aromatic rings.

**Conformational Control by NH···$\pi$ Interactions.** Since the results obtained for the macrocycles **1a**,**b** and **2a**,**b** suggested the participation of NH···$\pi$ interactions in the conformational stability of the compounds, we envisioned other derivatives to demonstrate the utility of this effect to design a preferred conformation and folding of the structures. We used **1b** as the starting point because it showed the more efficient NH···$\pi$ interaction by molecular modeling and VT-NMR (largest entropic contribution to the energetic barrier). With this aim, we synthesized **1c** and *meso*-**1b** (Scheme 2), which can be seen as variations of the previously studied **1b**. Thus, **1c** would be

(26) Becerril, J.; Bolte, M.; Burguete, M. I.; Galindo, F.; García-España, E.; Luis, S. V.; Miravet, J. F. *J. Am. Chem. Soc.* **2003**, *125*, 6677−6686.

(27) All the molecular modeling was performed using: *Spartan '04*; Wavefunction, Inc.: Irvine, CA, 2004. For MMFF force field calculations, see: Halgren, T. A. *J. Comput. Chem.* **1996**, *17*, 490−519 and the other papers in this issue. For quantum mechanics calculations, see: Kong, J.; White, C. A.; Krylov, A. I.; Sherrill, D.; Adamson, R. D.; Furlani, T. R.; Lee, M. S.; Lee, A. M.; Gwaltney, S. R.; Adams, T. R.; Ochsenfeld, C.; Gilbert, A. T. B.; Kedziora, G. S.; Rassolov, V. A.; Maurice, D. R.; Nair, N.; Shao, Y.; Besley, N. A.; Maslen, P. E.; Dombroski, J. P.; Daschel, H.; Zhang, W.; Korambath, P. P.; Baker, J.; Byrd, E. F. C.; van Voorhis, T.; Oumi, M.; Hirata, S.; Hsu, C.-P.; Ishikawa, N.; Florian, J.; Warshel, A.; Johnson, B. G.; Gill, P. M. W.; Head-Gordon, M.; Pople, J. A. *J. Comput. Chem.* **2000**, *21*, 1532−1548.

(28) (a) Li, X.; Yang, D. *Chem. Commun.* **2006**, 3367−3379. (b) Jimenez, A. I.; Ballano, G.; Cativiela, C. *Angew. Chem., Int. Ed.* **2005**, *44*, 396−399. (c) Vass, E.; Hollósi, M.; Besson, F.; Buchet, R. *Chem. Rev.* **2003**, *103*, 1917−1954. (d) Guruprasad, K.; Rao, M. J.; Adindla, S.; Guruprasad, L. *J. Pept. Res.* **2003**, *62*, 167−174. (e) Improta, R.; Barone, V.; Kudin, K. N.; Scuseria, G. E. *J. Am. Chem. Soc.* **2001**, *123*, 3311−3322. (f) Marraud, M.; Aubry, A. *Biopolymers* **1996**, *40*, 45−83. (g) Rose, G. D.; Gierasch, L. M.; Smith, J. A. *Adv. Protein Chem.* **1985**, *37*, 1−109. (h) Toniolo, C. *Crit. Rev. Biochem.* **1980**, *9*, 1−44.

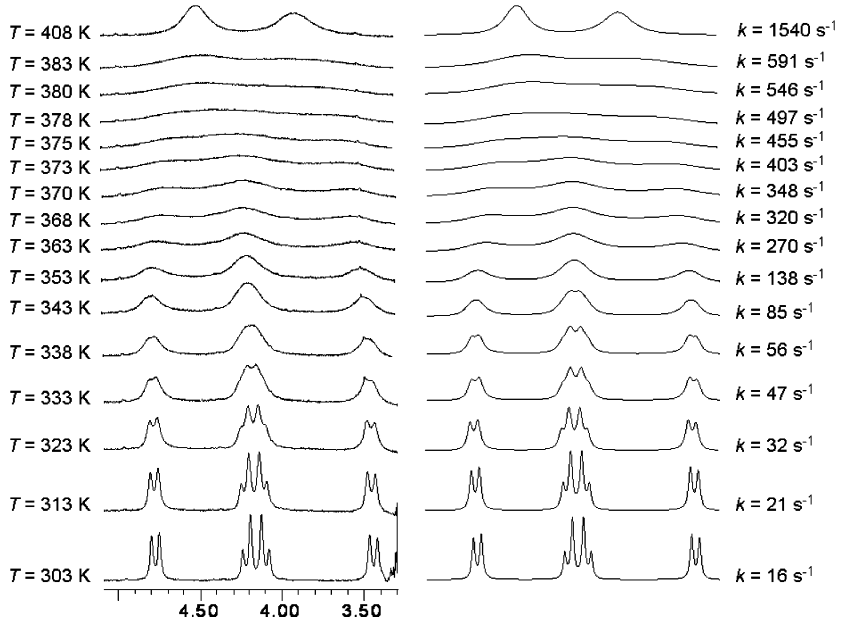


**FIGURE 2.** Partial (protons at C2 carbon) VT-NMR spectra of **1a** (5 mM, DMSO-$d_6$, 300 MHz): experimental (left) and simulated (right). Values of temperature ($T$, K) and interconversion rate ($k$, $s^{-1}$) are also given for every trace. Simulated spectra were obtained with the gNMR program.[23]

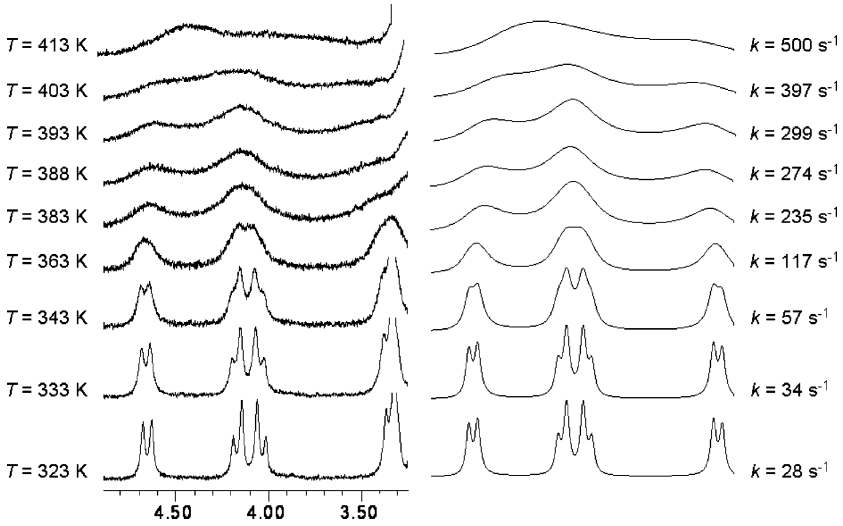


**FIGURE 3.** Partial (protons at C2 carbon) VT-NMR spectra of **1b** (5 mM, DMSO-$d_6$, 300 MHz): experimental (left) and simulated (right). Values of temperature ($T$, K) and interconversion rate ($k$, $s^{-1}$) are also given for every trace. Simulated spectra were obtained with the gNMR program.[23]

**TABLE 2. Activation Parameters for 1a,b and 2a**

| entry | compd | $E_a$ (kcal/mol)[a] | $\Delta H^{\ddagger}$ (kcal/mol)[a] | $\Delta S^{\ddagger}$ (cal $K^{-1}$ $mol^{-1}$)[b] | $\Delta G^{\ddagger}_{(298)}$ (kcal/mol)[a] | solvent |
|---|---|---|---|---|---|---|
| 1 | **1a** | 11.5 | 10.8 | −18.3 | 16.2 | DMSO-$d_6$ |
| 2 | **1b** | 8.9 | 8.1 | −27.0 | 16.2 | DMSO-$d_6$ |
| 3 | **2a** | 9.7 | 9.1 | −15.3 | 13.7 | $CDCl_3$ |

[a] Estimated error ±0.15 kcal/mol. [b] Estimated error ±0.5 cal $K^{-1}$ $mol^{-1}$.

the result of the elimination of one phenyl ring in one side chain of **1b**, while *meso*-**1b** was designed to check the effect of spatial disposition of side chains. Additionally, since the pseudopeptidic chain has been constructed by the assembly of two different amino acids (Phe and Ala for **1c** or D/L-Phe for *meso*-**1b**), the average $C_2$ symmetry in the fast exchange regime was broken. As a consequence, the flipping proposed on these derivatives (Scheme 2) would produce two different diastereoisomers regarding the planar chirality of the naphthalenophane.

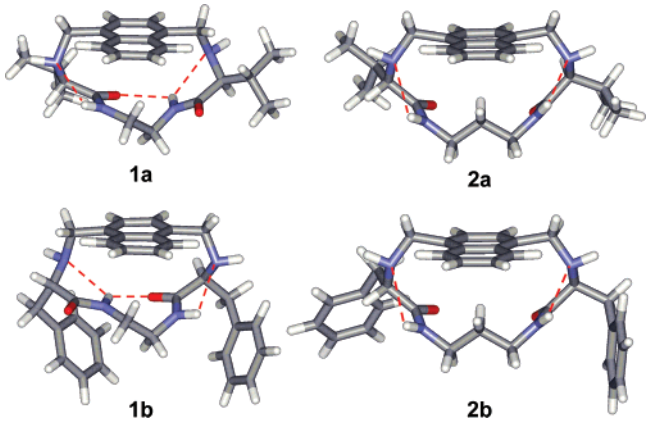


**FIGURE 4.** Minima of energy for **1a**,**b** and **2a**,**b**. Hydrogen bonding interactions are red dashed lines.

**SCHEME 2. Molecular Structures and Proposed Conformational Equilibria for 1c and *meso*-1b**

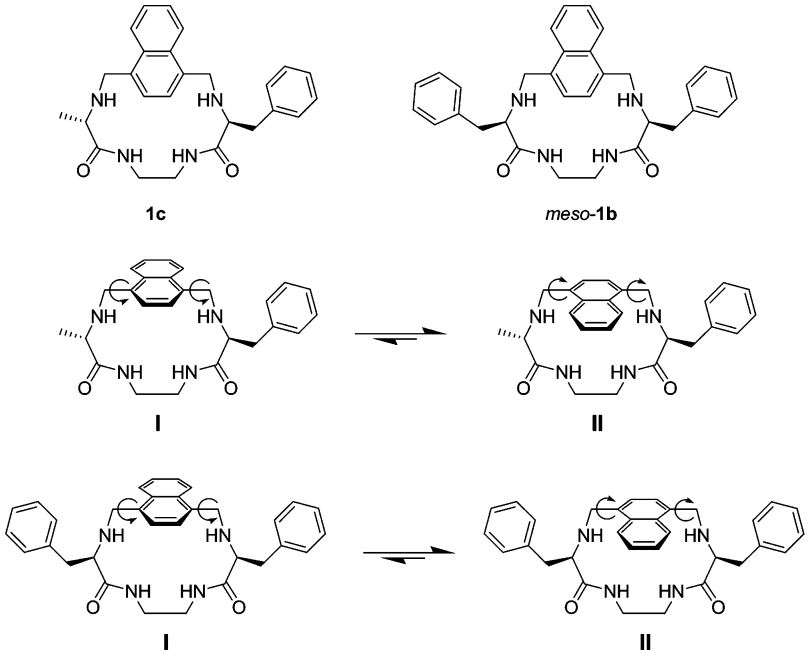


One of them would set the naphthalene and the aromatic side chains in opposite sides of the macrocycle (anti or type I in Scheme 2), and the other would locate both aromatic groups toward the same macrocyclic face (syn or type II in Scheme 2). As the energy barrier for the inversion of the 16-membered ring is expected to be similar to those measured for **1a**,**b**, both diastereomers (I and II) will interconvert slowly in the NMR time scale, making their corresponding $^1$H NMR signals observable at room temperature. Besides, these two diastereoisomers would display different abilities to set the proposed NH$\cdots\pi$ interactions, as a consequence of the geometrical disposition of the naphthyl and phenyl groups. Taking this into account, we anticipated the *syn*-II isomer to be favored, its relative stability being an indirect measurement of the role of NH$\cdots\pi$ interactions in the folding of the model compounds.

According to our design, the $^1$H NMR spectrum of **1c** showed a complicated group of signals as an indication of the presence of two species in solution, which were characterized by bidimensional COSY, TOCSY, and NOESY experiments (Supporting Information). Detailed analysis of the 2-D NOESY spectrum confirmed the presence of both rotamers I and II connected through EXSY cross-peaks (Supporting Information) and allowed the partial assignment of their corresponding proton signals. Careful integration of some of these signals rendered a 2:3 mole ratio of I/II diastereoisomers (500 MHz, 303 K, DMSO-$d_6$). This would mean that $\Delta G_{(303K)} = 0.25$ kcal/mol favorable to the *syn*-II isomer. Additionally, we estimated from VT-NMR experiments the energetic barrier for the interconversion to be $\Delta G^{\ddagger}_{(373K)} = 19.2$ kcal/mol, in good agreement with that observed for **1b**. Monte Carlo conformational searches[27] on **1c** also showed *syn*-II as a more stable conformation than *anti*-I, although the computed energetic difference (MMFF force field) was much higher than the experimental one. However, the energy minima thus obtained also show the H-bonding pattern and NH$\cdots\pi$ interactions previously found for **1b** (Supporting information). Thus, both experimental NMR data and modeling reflect the preference of the aromatic rings to set to the same face of the macrocycle, probably interconnected through aryl−NH−aryl contacts.

Fortunately, NMR analysis of *meso*-**1b** was even more illustrative, as its $^1$H NMR spectrum showed a unique, very simple, and symmetric structure in solution (both in DMSO-$d_6$ and in $CDCl_3$), which remains unaltered up to 403 K (300 MHz, DMSO-$d_6$), suggesting a very stable conformation. With the help of a full set of 1-D NOESY experiments, we were able to unambiguously assign this species to be the *syn*-II diastereomer (Figure 7). For instance, selective irradiation on H9 produced NOE enhancements on H10, amide NH, and one of the diastereotopic protons on C2, H2A. On the other hand, irradiation on the diastereotopic counterpart, H2B, produced a NOE effect on H7 and H3, the C$\alpha$ proton. Besides, the amide NH proton resonates at low chemical shifts (Figure 5), due to the shielding effect of the anisotropy cones of the aromatic rings. These data confirm that both aromatic groups point toward the same face of the macrocyclic ring and that the amide group is close to the naphthalene ring, thus preventing solvent accessibility to the NH protons. Regarding that, the temperature factor of the amide NH chemical shift in DMSO-$d_6$ was found to be notably small, $\Delta\delta NH/\Delta T = -2.30$ ppb/K.[29] Besides, the chemical shift difference of this $^1$H NMR signal in $CDCl_3$ or DMSO-$d_6$ [$\delta$(DMSO-$d_6$) − $\delta$($CDCl_3$) = 0.39 ppm] was also small. All these data support the existence of a strong intramolecular hydrogen bond pattern even in a very competitive solvent and a poor solvent accessibility to the amide NH protons, in good agreement with the proposed conformation and our initial design.

This structural arrangement was also obtained by molecular modeling studies[27] (Monte Carlo search and MMFF force field minimization), which showed the preference of the macrocycle to adopt the *syn*-II structure, being 3.5 kcal/mol more stable than the *anti*-I diastereoisomer (Figure 6A and Table 3). The minimum found for *syn*-II also showed internuclei distances in

(29) It was not possible to accurately measure the corresponding amide NH temperature factor for all the other compounds due to exchange produced by ring inversion. (a) Alonso, E.; López-Ortiz, F.; Del Pozo, C.; Peralta, E.; Macías, A.; González, J. *J. Org. Chem.* **2001**, *66*, 6333−6338. (b) Belvisi, L.; Gennari, C.; Mielgo, A.; Potenza, D.; Scolastico, C. *Eur. J. Org. Chem.* **1999**, 389−400.

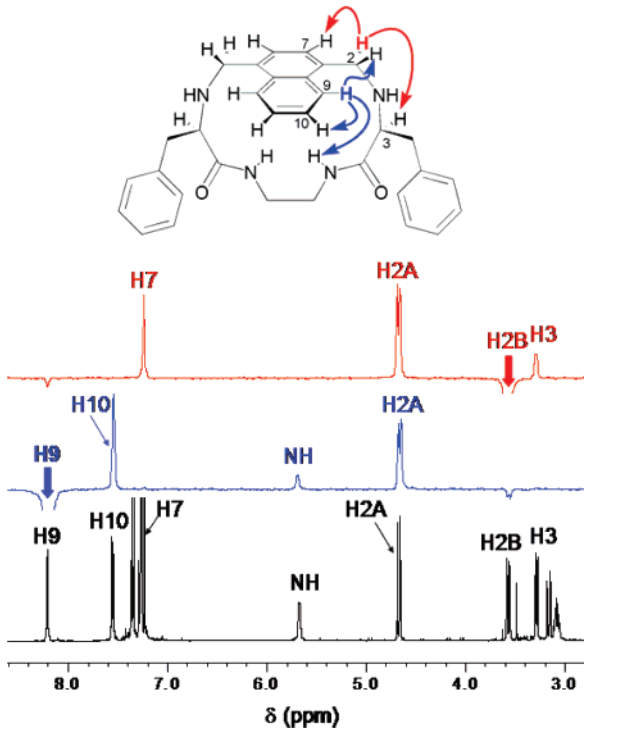


**FIGURE 5.** Selected 1-D NOESY experiments (500 MHz, 303 K, $CDCl_3$) of *meso*-**1b** obtained by selective pulse field gradient irradiation (bold arrow) on H9 (blue trace) or H2B (red trace).

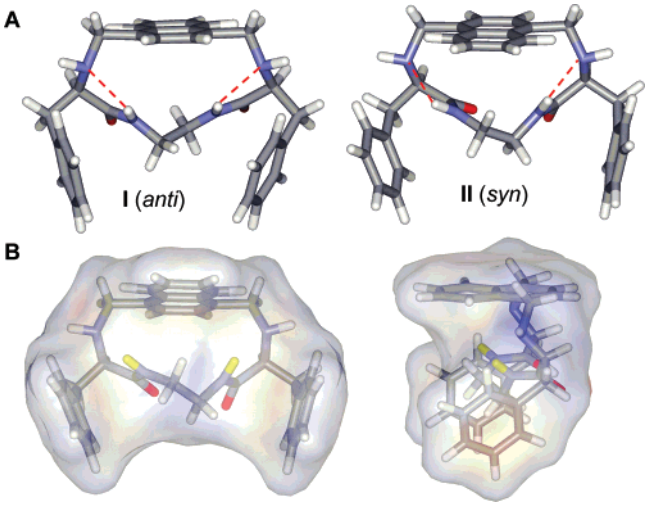


**FIGURE 6.** (A) Minimized structures for *anti*-I and *syn*-II diastereoisomers of *meso*-**1b**, with hydrogen bonds as red dashed lines. (B) Front and side views of *syn*-II geometry displaying the solvent-accessible surface. The solvent excluded amide NH protons are in yellow.

agreement with the experimental NOEs and presented two intramolecularly H-bonded amide protons, surrounded by the aromatic rings. A careful analysis of the structural differences between both geometries (I and II) showed a closer contact of the amide hydrogen atoms with the naphthyl ring for the *syn*-II isomer (Table 3). Consequently, the theoretical calculations nicely reflect the stabilization effect of the amide NH−aryl contacts and also give an explanation for the complete diastereoselectivity obtained in solution.

Also, in this case, we tried to qualitatively study the solvent exposure of the amide NH protons in the most stable conformation by computing the solvent-accessible surface (Figure 6B). In this conformation, the aromatic rings create an electron-rich desolvated cavity, perfectly suited to host the intramolecular H-bonded amide NH group. This calculation agrees with both the low chemical shift and the temperature factor of NH protons in a highly competitive solvent, such as DMSO.

We have performed additional theoretical calculations to understand the nature of the NH···$\pi$ contacts in our most efficient model, *meso*-**1b**, in spite of the controversial debate about the origin of weak interactions.[30] Previous theoretical calculations[31] found that amide−aromatic interactions mainly emerge from a combination of dispersion and electrostatic forces, which both have an electronic origin. Then, we optimized the system using more accurate DFT quantum calculations at the B3LYP/6-31G(d) level of theory. Full optimization of both diastereoisomers of *meso*-**1b** yielded two minima with geometries only slightly different from those obtained by MMFF force field calculations and characterized by the disposition of the amide NH bonds perpendicular to the naphthalene main plane (Figure 7A). These T-shaped geometries maximize the attractive interaction between the electric dipole of the amide groups and the quadrupole of the aromatic ring, and they are expected to be favored by quantum calculations in the gas phase. Interestingly, DFT calculations rendered a closely similar energy difference, $\Delta E = 3.7$ kcal/mol, favorable to the *syn*-II diastereoisomer, in good agreement with the molecular mechanics approach. Thus, the MMFF force field seems to reflect the NH···$\pi$ interactions in a reasonable fashion, at least for a first approximation. On the other hand, the DFT energy difference would render a population of >99% of the *syn*-II isomer up to 403 K, in a perfect agreement with the observation of only this rotamer by VT-NMR experiments within our accessible temperature range.

To better visualize the NH···$\pi$ stabilizing contacts, we used two different graphical representations. First of all, the CPK model of the minimum found for the *syn*-II isomer of *meso*-**1b** at the B3LYP/6-31G(d) level of theory showed clear van der Waals contacts between both the amide NH atoms and the aromatic $\pi$-cloud of the naphthyl ring (Figure 7B). This observation follows the existence of dispersion forces between both moieties of the system. A further representation of the weak NH···$\pi$ interactions can be performed using the electron density of the whole molecule, available from the electronic configuration obtained by the B3LYP/6-31G(d) calculations.[32] As this stabilizing contact has an important electrostatic contribution, we mapped the electrostatic potential (ESP) onto the global electron density surface, different contours being evaluated for illustrative purposes.[33] The electron-rich areas (mainly $\pi$-electron densities and electron lone pairs) are qualitatively represented in red, while the electron-poor areas (mainly polarized hydrogen atoms) are in blue. Electron density surfaces at different isosurface values (Isoval) are shown in Figure 7C. The electron density isosurface at Isoval = 0.002 au represents >98% of the electronic charge and reflects a close similarity to the CPK

(30) Dunitz, J. D.; Gavezzotti, A. *Angew. Chem., Int. Ed.* **2005**, *44*, 1766−1787.
(31) Duan, G.; Smith, V. H., Jr.; Weaver, D. F. *J. Phys. Chem. A* **2000**, *104*, 4521−4532.
(32) Hehre, W. J. *A Guide to Molecular Mechanics and Quantum Chemical Calculations*; Wavefunction Inc.: Irvine, CA, 2003.
(33) This approach has been very recently used to study sugar−aromatic weak interactions: Terraneo, G.; Potenza, D.; Canales, A.; Jiménez-Barbero, J.; Baldridge, K. K.; Bernardi, A. *J. Am. Chem. Soc.* **2007**, *129*, 2890−2900.

**TABLE 3. Selected Structural Data of the Two Minimized Geometries (MMFF) Found for *meso*-1b**

| structure | H atom | *d*[N−H···N][a] | *d*[N−H···Ph][b] | *d*[N−H···Nap][b] | *E* (kcal/mol)[c] |
|---|---|---|---|---|---|
| *anti*-I | (*R*)−C$^{\alpha}$−CON*H* | 2.37 | 2.95 | 2.85 | 129.6 |
| | (*S*)−C$^{\alpha}$−CON*H* | 2.38 | 2.89 | 2.87 | |
| | av[d] | 2.38 | 2.92 | 2.86 | |
| *syn*-II | (*R*)−C$^{\alpha}$−CON*H* | 2.41 | 2.81 | 2.84 | 126.1 |
| | (*S*)−C$^{\alpha}$−CON*H* | 2.28 | 3.07 | 2.69 | |
| | av[d] | 2.35 | 2.94 | 2.74 | |

[a] Distance (Å) from amide H to the amino nitrogen, forming a five-membered ring. [b] Distance (Å) from amide H to the center of the closest aryl C−C bond. [c] Computed energy using the MMFF force field implemented in Spartan 04. [d] Averaged value (Å) between both amide hydrogen atoms.

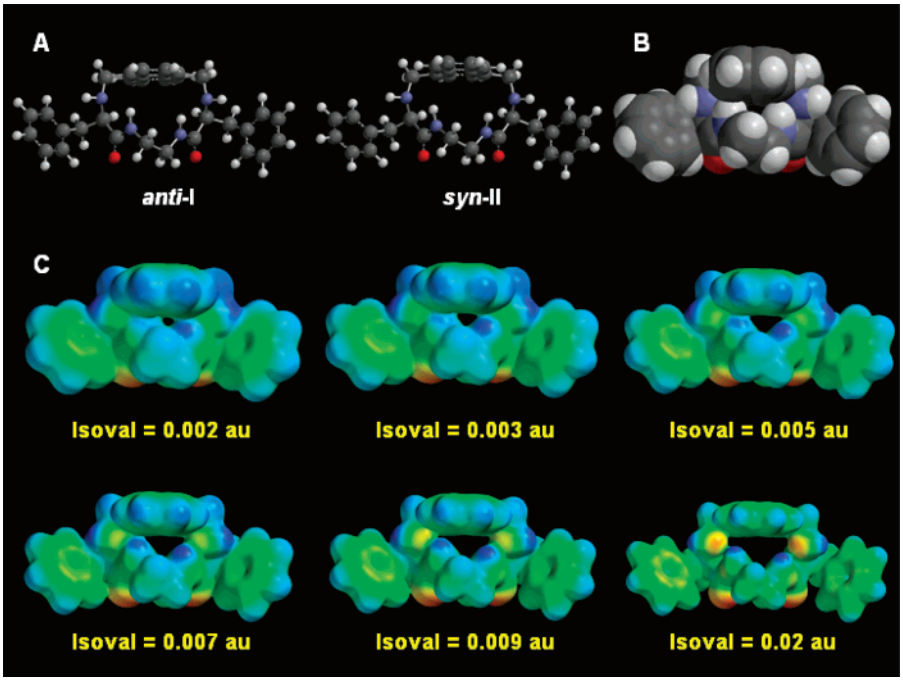


**FIGURE 7.** (A) Minimized B3LYP/6-31G(d) geometries for both diastereoisomers of *meso*-**1b**. (B) CPK model for *syn*-II diastereoisomer. (C) ESP mapped onto the global electron density [B3LYP/6-31G(d)] at different isosurface values (Isoval) for the *syn*-II minimum of *meso*-**1b**.

representation. The relative ESP around the amide protons clearly indicates contact with the naphthalene ring, confirming their mutual bonding interaction. The surface at Isoval = 0.003 au, encompassing a smaller electron density and accordingly closer to the nucleus, still shows important overlapping between both NH groups and naphthyl moieties. The contact with one of the amide NH atoms is lost at Isoval = 0.005 au, suggesting a lower limit of ca. 3.1 kcal/mol for the energy of the interaction with both groups. The isosurface at 0.007 showed the contact of naphthalene with only one of the amide protons. Moving yet closer to the nucleus, at Isoval = 0.009 au, no contact between the amide NH groups and the naphthyl ring was observed. Interestingly, we have to move much closer to the nucleus, at Isoval = 0.02 au, to eliminate the amide−amine intramolecular H-bond, highlighting that this interaction is stronger than the amide NH···$\pi$ contact. Besides, this analysis allowed an estimation of the extent of the NH···$\pi$ interactions in this system, located within 0.005−0.009 au or 3.1−5.6 kcal/mol. These values are in good agreement with our experimental and theoretical results, as well as with published calculations on benzene−formamide complexes.[31]

## Conclusion

The conformational behavior of 16- and 17-membered ring macrocyclic naphthalenophanes (**1a**,**b** and **2a**,**b**) derived from amino acids (Val and Phe) has been studied by VT-NMR and molecular modeling. The flipping rate of the naphthalene moiety occurs within the NMR time scale range, which has allowed us to deeply study this dynamic process. From the VT-NMR experiments, clear tendencies have been observed depending on the macrocyclic ring size and, more interestingly, the nature of the side chain of the peptidomimetic fragment. In general, macrocycles bearing aromatic side chains tend to be less flexible related to the ring inversion process. The negative values of $\Delta S^{\ddagger}$ are noteworthy, which is most likely due to a higher solvation of the TS as compared to the GS. This observation is especially important for the derivatives bearing aromatic side chains. Molecular modeling suggested the participation of amide NH···$\pi$ interactions on the preferred conformations, which lead to a more efficient desolvation of the pseudo-peptidic moiety due to the presence of aromatic rings.

To confirm our proposal, we designed and prepared new derivatives (**1c** and *meso*-**1b**) in which the flipping process would lead to different diastereoisomers regarding the planar chirality of the naphthalenophane ring. Careful NMR analysis of these derivatives confirmed the major presence of the corresponding rotamers showing both aryl groups (naphthyl and benzyl) toward the same side of the macrocyclic main plane, surrounding the peptidic NH bonds. This stereoselectivity is moderate for **1c** but complete for *meso*-**1b**. The $^{1}$H NMR data

for *meso*-**1b** in different solvents and temperatures suggested that amide NH is implicated in a strong intramolecular hydrogen bond and immersed in a desolvated environment. Besides, molecular mechanics showed good agreement with experimental results and confirmed the participation of amide NH$\cdots\pi$ interactions in the stabilization of the major diastereoisomers. Further DFT quantum mechanics calculations were also performed, showing a very good agreement with both experimental and MMFF data. The combination of CPK models and ESP analysis onto the electron density surfaces allowed us to characterize this NH$\cdots\pi$ stabilizing contact as a combination of dispersion and electrostatic interactions. By the combination of all theoretical and experimental data, we limit this interaction within the energetic range of 3.1−5.6 kcal/mol.

The study of amide NH$\cdots\pi$ interactions in model systems is of great interest for the understanding of these noncovalent contacts in biological chemistry and molecular recognition processes. From our studies, we found that both dispersion and electrostatic interactions contribute to the bonding stabilization energy, with solvent exclusion playing a fundamental role. Besides, their use to induce a highly diastereoselective conformational preference is, as far as we know, unprecedented. Indeed, the cooperative operation of NH$\cdots\pi$ weak interactions and solvent exclusion make one of our simple models (*meso*-**1b**) to exclusively fold into one of the possible diastereomeric geometries, in the same manner as biomolecules often behave in nature.

## Experimental Section

Compounds **1a**,**b** and **2a**,**b** were synthesized as previously described,[34] while **1c** and *meso*-**1b** were prepared in a similar way, by performing a macrocyclization reaction from the corresponding open chain bis(amidoamine). More detailed descriptions of the synthesis and characterization of **1c** and *meso*-**1b** are given in the Supporting Information. For the VT-NMR experiments, samples were prepared by weighing the necessary amount of peptidomimetic naphthalenophane and adding a known volume (typically 0.7 mL) of the desired deuterated solvent. The final concentration was 5−10 mM in all the cases. To take advantage of the magnetic field value, measurements requiring temperatures higher than room temperature for observing coalescence were performed in an apparatus with a proton resonance frequency of 300 MHz. Conversely, when cooling was necessary to achieve decoalescence, a 500 MHz (also for $^1$H NMR) magnetic field was used. The temperature of each NMR spectrometer was calibrated by the methanol method in separate experiments.[35] The accuracy in the temperature measurement was at least ±1 K. The reversibility of the changes produced in NMR signals was checked by repeated measuring at different temperatures. The approximated values of the free energy of activation ($\Delta G^{\ddagger}_c$) at the coalescence temperature ($T_c$) were obtained from the following formula: $\Delta G^{\ddagger} = RT_c[22.96 + \ln(T_c/\delta\nu)]$.[22] Fitting of dynamic NMR line shapes at different temperatures was performed with the gNMR program.[23] The activation parameters were calculated by the least-squares fitting of suitable plots of the corresponding kinetic values obtained from the line-shape analysis and the measured temperatures of the experimental spectra. As the simulation could be carried out at several temperatures (eight or more), the estimated error in $\Delta G^{\ddagger}$ is about ±0.15 kcal/mol.[36] To obtain the minima of energy by molecular modeling, the conformer distribution calculation option available in Spartan '04 was used.[27] With this option, an exhaustive Monte Carlo search without constraints was performed for every structure. The torsion angles were randomly varied, and the obtained structures were fully optimized using the MMFF force field. Thus, 100 minima of energy within an energy gap of 10 kcal/mol were generated. These structures were analyzed and ordered considering the relative energy, the repeated geometries being eliminated. When different diastereoisomers were possible (**1c** and *meso*-**1b**), we calculated both rotamers separately to ensure the complete mapping of the conformational energy hypersurface. For DFT calculations at the B3LYP/6-31G(d) level of theory, full minimization and frequency analysis were performed with Spartan '04.[27] The ESP mapped onto the global electron density surfaces was computed at Isoval = 0.002, 0.003, 0.004, 0.005, 0.006, 0.007, 0.008, 0.009, 0.010, 0.015, and 0.020 au using the B3LYP/6-31G(d) wavefunction and with the facilities also available in this package. The graphics of the CPK model and ESP electron densities represented in Figure 7 were displayed using Spartan '04.[27]

**Acknowledgment.** This paper is dedicated to Prof. Vicente Gotor on the occasion of his 60th birthday. Financial support from the Spanish Ministerio de Educación y Ciencia (CTQ2006-15672-C05-02) and Bancaixa-UJI (P11B2004-38) is gratefully acknowledged. I.A., F.G., and L.V. also thank MEC for financial support (Ramón y Cajal program for I.A. and F.G. and predoctoral F. P. U. fellowship for L.V.).

**Supporting Information Available:** Experimental synthetic details and characterization, including copies of $^1$H NMR, $^{13}$C NMR, and gCOSY spectra for *meso*-**1b** and $^1$H NMR, $^{13}$C NMR, gCOSY, TOCSY, and NOESY spectra for **1c** (3:2 *syn*/*anti* diastereomeric mixture); experimental and simulated partial NMR spectra for the VT-NMR analysis; Arrhenius and Eyring plots; computed solvent-accessible surfaces for **1a**,**b**; and *XYZ* coordinates and energies of the geometries for all obtained global minima. This material is available free of charge via the Internet at http://pubs.acs.org.

JO701552B

(34) Burguete, F; Galindo, F.; Izquierdo, M. A.; Luis, S. V.; Vigara, L. *Tetrahedron* **2007**, *63*, 9493−9501.

(35) Braun, S.; Kalinowski, H.-O.; Berger, S. *150 and More Basic NMR Experiments*; Wiley-VCH: Weinheim, Germany, 1988.

(36) Bonini, B. F.; Grossi, L.; Lunazzi, L. *J. Org. Chem.* **1986**, *51*, 517−522.